ELSEVIER

Journal of Alloys and Compounds 335 (2002) 254–261

Journal of ALLOYS AND COMPOUNDS

www.elsevier.com/locate/jallcom

Martensitic transformation of a Ti-rich $Ti_{51}Ni_{47}Si_2$ shape memory alloy☆

S.F. Hsieh[a], S.K. Wu[b,*], H.C. Lin[c]

[a]*Department of Mold and Die Engineering, National Kaohsiung University of Applied Science, Kaohsiung, Taiwan 807, ROC*
[b]*Institute of Materials Science and Engineering, National Taiwan University, 1 Roosevelt Rd., Sec. 4, Taipei, Taiwan 106, ROC*
[c]*Department of Materials Science, Feng Chia University, Taichung, Taiwan 407, ROC*

Received 25 April 2001; accepted 21 August 2001

Abstract

$Ti_{51}Ni_{47}Si_2$ alloy is similar to $Ti_{51}Ni_{49}$ alloy with nearly equal transformation temperatures and having B2↔19′ martensitic transformation. Despite the existence of many second phase particles, this alloy still exhibits good shape recovery. The B19′ martensite structure in $Ti_{51}Ni_{47}Si_2$ alloy is calculated from SADPs as $a=0.284$ nm, $b=0.412$ nm, $c=0.468$ nm and $\beta=98°$. Martensitic transformation temperatures decrease with increasing aging time at 400°C. The hardness increment and transformation temperature depression of $Ti_{51}Ni_{47}Si_2$ alloy are more than those of $Ti_{51}Ni_{49}$ alloy under the same degree of cold rolling and the same number of thermal cycles due to the former alloy having a higher inherent hardness from Si atoms solid-soluted in TiNi alloy. The strengthening effects of cold rolling and thermal cycling on M_s temperature of $Ti_{51}Ni_{47}Si_2$ alloy follow the expression of $M_s=T_o-K\Delta\sigma_y$.

Keywords: Transition metal alloys; TEM; Phase transition; Mechanical properties

1. Introduction

Near-equiatomic TiNi alloys are among the most important shape memory alloys (SMAs) due to their superior shape memory effect and superelastic properties. The application of these alloys has spread not only to engineering but also to medical and dental fields. It has been confirmed that TiNi SMAs' properties can be affected by various thermal–mechanical treatments, such as thermal cycling [1], aging treatment in Ni-rich alloys [2–4] and cold rolling [5]. Furthermore, the addition of a third element has a substantial effect on phase transformation behavior in TiNi SMAs. The M_s temperature decreases monotonously following substitution of Ni with V, Cr, Mn, Fe and Co elements [6–9], but increases remarkably following substitution of Ni with Au, Pd and Pt in amounts not less than 15–20 at.% [10–12]. The transformation sequence of TiNi-based SMAs can be B2→R→B19′ for TiNiFe, TiNiAl and TiNiCo alloys [9,13,14], but B2→B19→B19′ for TiNiCu and TiNiPd alloys [15,16] under different thermal–mechanical processes composed of a high temperature cubic B2 phase, an intermediate rhombohedral R phase (or orthorhombic B19 phase) and a low temperature monoclinic B19′ phase.

TiNi thin films fabricated by r.f.-sputtering are considered to be promising candidates for microactuators due to their large deformation and strong recovery force. The sputtering TiNi thin film deposited on Si substrate is amorphous and does not behave as a SMA. Therefore, crystallization annealing is necessary [17]. However, if the annealing temperature is higher than 600°C, Ni and Si atoms diffuse across the interface of TiNi film and Si substrate and ternary silicides such as $Ti_1Ni_1Si_1$, $Ti_4Ni_4Si_7$ are formed at the interface [18]. At the same time, it is well-known that a small deviation from stoichiometry in TiNi SMAs can give rise to a significant precipitation of second phases [19,20]. This in turn affects both the alloy's strength and its shape memory effect. To our knowledge, transformation characteristics and precipitated second phases of TiNiSi ternary SMAs with small amounts of Si have not been reported yet. In this paper, we aim to investigate the transformation behavior of a Ti-rich $Ti_{51}Ni_{47}Si_2$ alloy. The effects of aging, cold rolling and thermal cycling on the martensitic transformation of $Ti_{51}Ni_{47}Si_2$ alloy are also discussed.

☆This manuscript has not been published elsewhere nor has it been submitted for publication elsewhere.

*Corresponding author. Tel.: +886-2-2363-7846; fax: +886-2-2363-4562.

E-mail address: skw@ccms.ntu.edu.tw (S.K. Wu).

0925-8388/02/$ – see front matter
PII: S0925-8388(01)01821-7

2. Experimental procedure

The conventional tungsten arc melting technique was employed to prepare $Ti_{51}Ni_{47}Si_2$ (in atomic percent) alloy. Titanium (purity 99.7 wt%), nickel (purity 99.9 wt%) and silicon (purity, 99.9 wt%), totaling about 100 g, were melted and remelted at least six times in an argon atmosphere. A pure titanium button was also melted and used as a getter. The mass loss during the melting was negligibly small. The as-melted buttons were homogenized holding at 950°C for 7 days and then quenched in water (the as-homogenized specimen). The buttons were cut into several plates with a low speed diamond saw, and then annealed at 900°C×2 h and quenched in water (the as-annealed specimen). After the annealing treatment, three experimental procedures were conducted. First, some plates were sealed in evacuated quartz tubes and aged at 400°C for 1–240 h and then quenched in water. Second, some plates were cold-rolled at room temperature to 5, 10, 20 and 25% reduction in thickness. Third, other plates were subjected to thermal cycling N times from 0 to 200°C with N=1–100 cycles. Specimens for DSC measurement, hardness testing, shape recovery test and microstructure observation were carefully cut from plates treated by the above procedures. DSC measurements were made with a Dupont thermal analyzer equipped with a quantitative scanning system 910 DSC cell for controlled heating and cooling runs on samples encapsulated in an aluminum pan. The running temperature range was from 0 to 200°C with a heating and cooling rate of 10°C/min. Specimens for the hardness test were first mechanically polished and then subjected to measurement in a Microvickers hardness tester with 500-g load at room temperature. For each specimen, the average hardness value was taken from at least five test readings. The microstructural observations were made by transmission electron microscopy (TEM) with a JOEL-100CXII microscope equipped with a conventional double-tilting stage. The shape-recovery measurement was performed as described earlier by Lin and Wu [21]. A quantitative analysis of chemical composition was carried out using a JOEL JXA-8600SX electron probe microanalyzer (EPMA) equipped with a WDX analysis system.

3. Experimental results and discussion

3.1. Transformation behavior

Fig. 1 shows the experimental results of DSC measurement for the homogenized $Ti_{51}Ni_{47}Si_2$ alloy, in both forward and reverse transformations, respectively. The peaks M* and A* appearing in Fig. 1 are associated with the first-order martensitic transformation of B2↔M.

Fig. 2 shows the EPMA backscattering electron image (BEI) of the as-homogenized $Ti_{51}Ni_{47}Si_2$ alloy. A great number of second phase particles are found around grain boundaries of the matrix. The chemical compositions of the matrix and second phase particles by EPMA analysis are shown in Table 1. The ratios Ti/(Ni+Si) of the matrix and second phase particles are also listed in Table 1. Based on the 750°C Ti–Ni–Si ternary phase diagram proposed by Markiv et al. [22], the results of Table 1 indicate that the matrix in Fig. 2 is Ti(Ni,Si) phase, the black particles are Ti_2(Ni,Si) phase and the gray particles are χ phase. The composition of the χ phase ($Ti_5Ni_4Si_1$) is in the range of 50–55 at.% Ti and 8–15 at.% Si. In this analysis, we suggest that the 750°C Ti–Ni–Si isotherm diagram is still suitable for the 950°C homogenized specimen. The volume fraction of second phase particles in $Ti_{51}Ni_{47}Si_2$ alloy is about 6%, which is nearly equal to that in $Ti_{51}Ni_{49}$ alloy.

It is reported that in as-quenched binary TiNi alloys, the As temperature increases with increasing linearly as the Ti

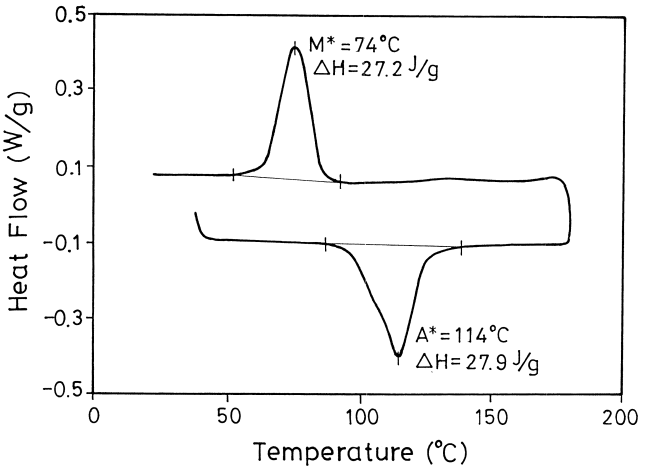

Fig. 1. DSC curves of as-homogenized $Ti_{51}Ni_{47}Si_2$ alloy. M* and A* are peak temperatures of forward and reverse martensitic transformation, respectively.

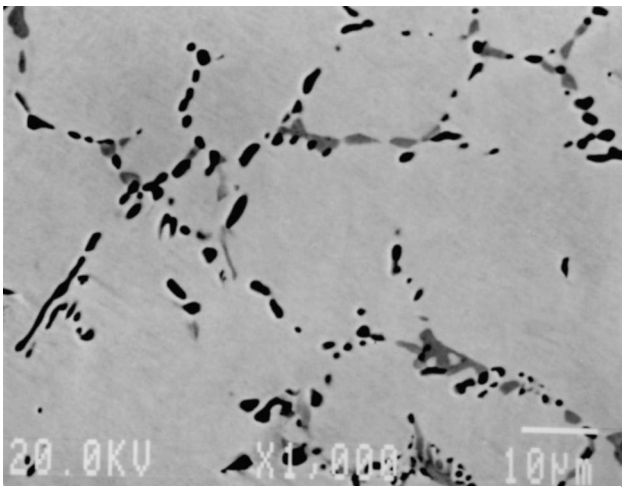

Fig. 2. EPMA backscattering electron image of as-homogenized $Ti_{51}Ni_{47}Si_2$ alloy.

Table 1
Compositional analyses by EPMA for $Ti_{51}Ni_{47}Si_2$ alloy homogenized at 950°C×7 days and then quenched

		Ti (at.%)	Ni (at.%)	Si (at.%)	Ti/(Si+Ni) ratio	Remark
$Ti_{51}Ni_{47}Si_2$	Matrix	51.21	47.96	0.83	1.05	Matrix
	Black particles	67.31	31.37	1.32	2.06	$Ti_2(Ni+Si)$
	Gray particles	50.12	34.49	15.39	–	χ-phase ($Ti_5Ni_4Si_1$)

content increases up to 50.5 at.% and then levels off at about 113°C [6]. The ratio, Ti/(Ni+Si), of the matrix in Fig. 2 is about 1.05, as shown in Table 1, which is nearly equal to the ratio Ti/Ni of $Ti_{51}Ni_{49}$ alloy. The peak temperatures A^* and M^* of $Ti_{51}Ni_{47}Si_2$ alloy shown in Fig. 1 are nearly equal to those of as-quenched $Ti_{51}Ni_{49}$ alloy [20]. This result indicates that a small amount of Si atoms solid-soluted in TiNi alloy has an equivalent effect to Ni atoms in Ti-rich $Ti_{51}Ni_{47}Si_2$ alloy.

Fig. 3(a) shows the TEM bright field image of martensite in the as-annealed $Ti_{51}Ni_{47}Si_2$ alloy. Fig. 3(b)–(d) are the selected area diffraction patterns (SADPs) of this alloy, with the foil being parallel to the $[100]_M$, $[010]_M$ and $[001]_M$ direction, respectively. Fig. 3(c) is taken from the martensite plates at the area E of Fig. 3(a) and $(001)_M$ compound twins can be observed. From the SADPs of Fig. 3(b) and (c), the lattice parameters of martensite in $Ti_{51}Ni_{47}Si_2$ alloy can be calculated as a monoclinic structure with $a=0.284$ nm, $b=0.412$ nm, $c=0.468$ nm and $\beta=98°$. From Figs. 1 and 3, one can find that the transformation sequence of martensite in $Ti_{51}Ni_{47}Si_2$ alloy is the B2↔B19′ one-stage transformation.

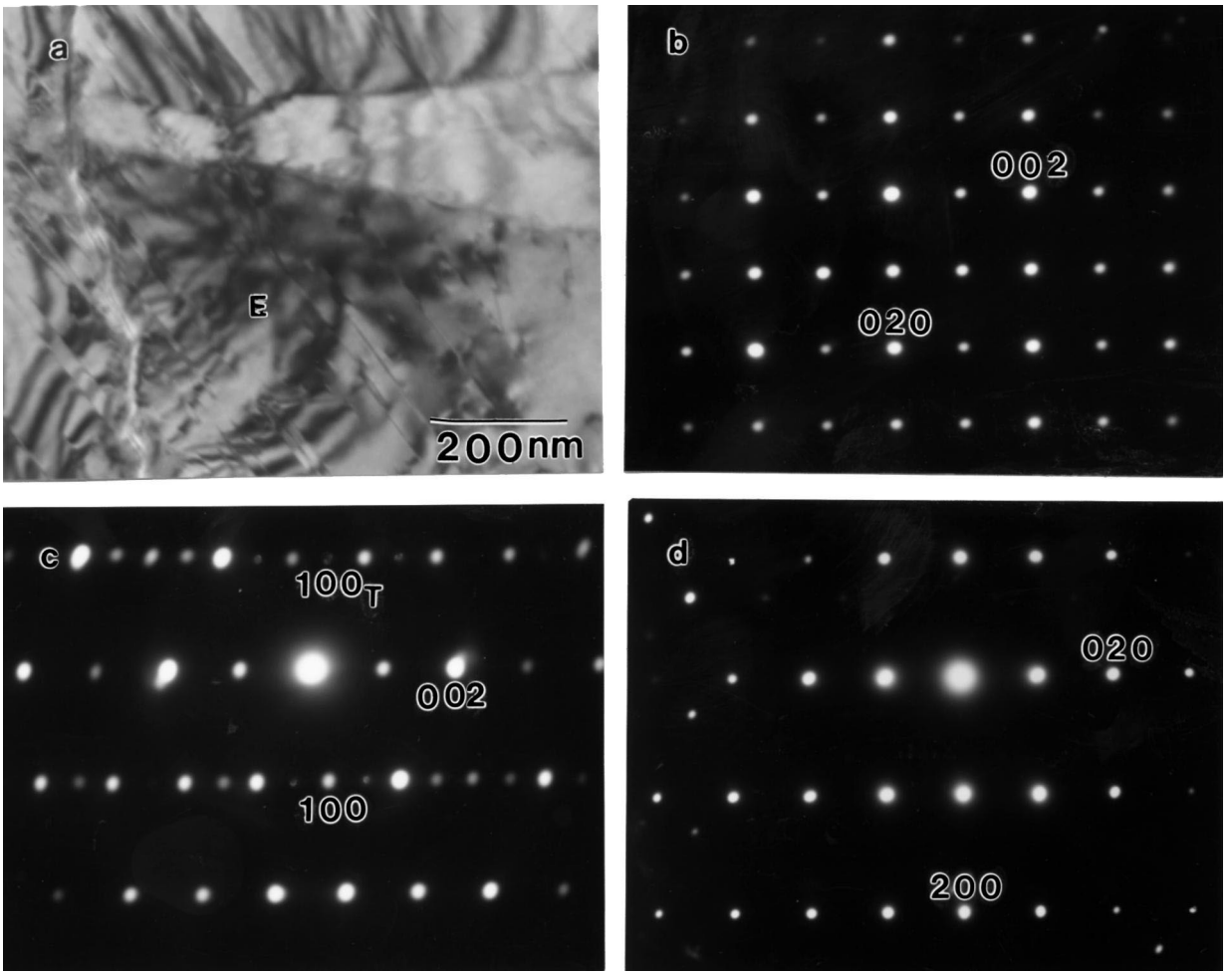

Fig. 3. (a) TEM bright-field image of as-annealed $Ti_{51}Ni_{47}Si_2$ alloy, (b) SADP of (a) with $[100]_M$ zone axis, (c) SADP taken from area E in (a), showing $(001)_M$ compound twins with $[010]_M$ zone axis, (d) SADP of (a) with $[001]_M$ zone axis.

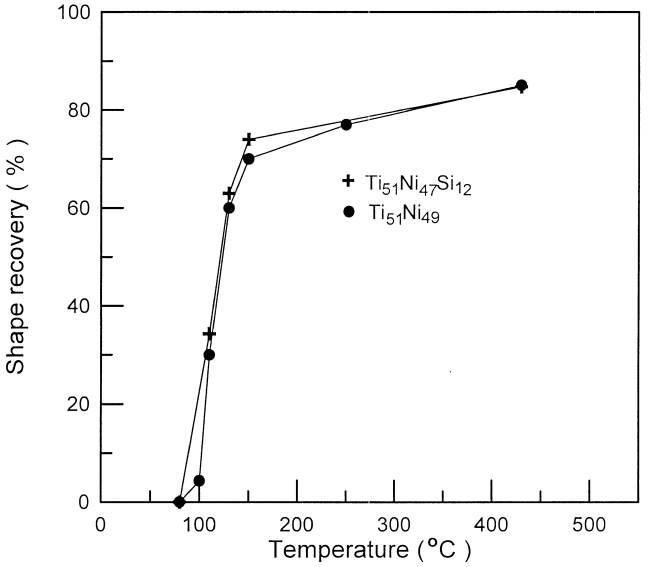

Fig. 4. Shape recovery versus heating temperature for the as-homogenized $Ti_{51}Ni_{47}Si_2$ and $Ti_{51}Ni_{49}$ alloys.

Fig. 4 shows the shape memory characteristics of $Ti_{51}Ni_{47}Si_2$ and $Ti_{51}Ni_{49}$ alloys. Despite the existence of many second phase particles, these alloys still exhibit good shape recovery that can reach about 85%. From Fig. 4, at the same temperature, the shape recovery of $Ti_{51}Ni_{47}Si_2$ alloy is slightly more than that of $Ti_{51}Ni_{49}$ alloy when the temperature is below 250°C, but both alloys exhibit nearly the same value when the temperature is above 250°C. This feature may result from the solid solution strengthening obtained by Si atoms solid-soluted in the TiNi B2 phase.

3.2. The aging effect

The DSC measurement for the 400°C aged $Ti_{51}Ni_{47}Si_2$ specimen shows that the transformation sequence is B2↔B19′ and the experimental *A** and *M** temperatures versus aging time are plotted in Fig. 5. The *A** and *M** temperatures gradually decrease with increasing aging time at 400°C. The hardness *Hv* of this aged alloy increases significantly in the first 48 h and then gradually levels off with further aging. The same characteristic shown in Fig. 5 also occurs in Ti-rich $Ti_{52}Ni_{47}Al_1$ and $Ti_{40.5}Ni_{49.5}Zr_{10}$ alloys [23,24], but does not appear in $Ti_{51}Ni_{49}$ alloy [20]. This characteristic can be explained as follows.

Based on the standard model for the solute diffusion in BCC lattices by a vacancy mechanism in dilute alloys [25], the excess quenched-in-vacancies can promote atomic rearrangement in TiNiX ternary alloys during the aging treatment at B2 phase in order to reduce the free energy of the system. This rearranged process in TiNiX alloys may introduce much more microstrain fields than that in TiNi binary alloys. In other words, a small Si addition to TiNi alloy can enhance the atomic rearrangement of dilute solute atoms during aging which can introduce lattice

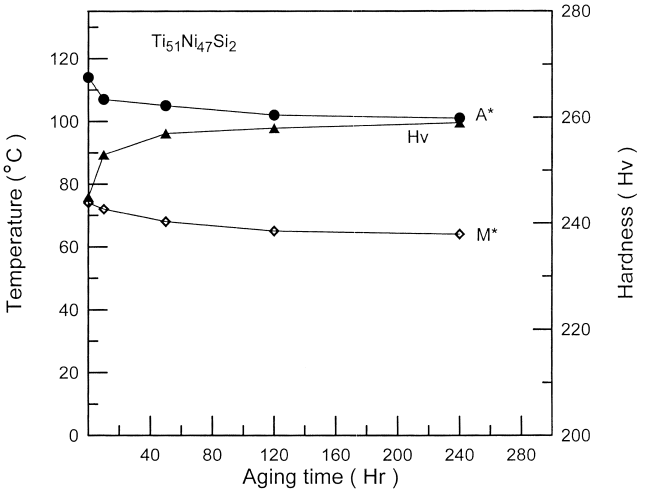

Fig. 5. The peak temperatures *A** and *M** and the hardness versus aging time for $Ti_{51}Ni_{47}Si_2$ alloy aged at 400°C.

distortion and hinder the mobility of twin plates in martensite/interface, leading to the transformation temperatures being depressed and the hardness being increased in aged TiNiX ternary alloys.

Fig. 6(a) shows the TEM bright-field image of B19′ martensite in a 400°C×240 h aged $Ti_{51}Ni_{47}Si_2$ alloy. Fig. 6(b) and (c) are the SADPs of Fig. 6(a) with the foil being parallel to $[111]_M$ and $[210]_M$ directions, respectively. Fig. 6(c) is taken from the martensite plate having fine striation at area B of Fig. 6(a). No extra reflection spot can be observed in Fig. 6(c) except the $(001)_M$ compound twins. Thus, the fine striations are traces of $(001)_M$ twins plates. Comparing Figs. 6 and 3, $(001)_M$ twin planes of the aged specimen are more dense than those of the annealed one. This result may indicate that $(001)_M$ compound twins of the aged specimen have a lower stacking fault energy than those of the annealed one.

3.3. The cold rolling effect

The effects of cold rolling on the martensite transformation of equiatomic TiNi binary alloy have been systematically studied and the martensite stabilization was observed in the cold-rolled TiNi martensite [5]. In this study, the $Ti_{51}Ni_{47}Si_2$ alloy underwent cold rolling at room temperature. Table 2 shows the detailed results of DSC and hardness measurements for various amounts of cold rolling (0–25%) in $Ti_{51}Ni_{47}Si_2$ alloy in which the A_1^* and A_2^* indicate the reverse transformation peaks of the first and second heating cycle for the specimen just after cold rolling. In Table 2, A_1^* temperature significantly increases, but A_2^* decreases, with increasing cold rolling. The *M** temperature is also found to decrease with increasing cold rolling. The above phenomenon is regarded as the mechanically-induced martensite stabilization in $Ti_{51}Ni_{47}Si_2$ alloy. The same behavior is also reported in Ti-rich $Ti_{51}Ni_{49}$ alloy [20]. After the occurrence of the first

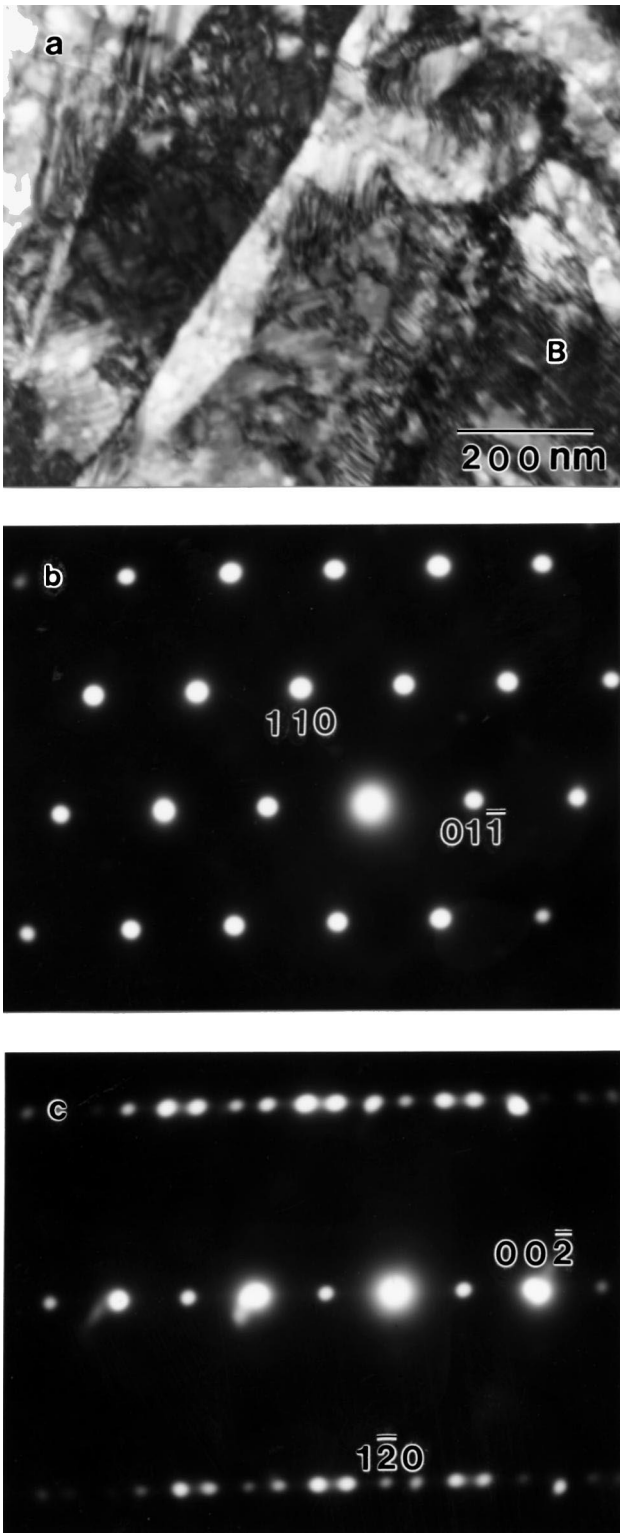

Fig. 6. (a) TEM bright-field image of martensite in $Ti_{51}Ni_{47}Si_2$ alloy aged at 400°C×240 h, (b) SADP of (a) with $[1\bar{1}\bar{1}]_M$ zone axis, (c) SADP taken from area B in (a), showing $(001)_M$ compound twins with $[210]_M$ zone axis.

reverse martensitic transformation B19′→B2, the martensite stabilization dies out and A_2^* temperatures are dramatically lowered. In Fig. 7(a), the difference between peak temperature A_1^* and A_2^*, ΔA^*, stands for the degree of martensite stabilization. From Fig. 7(a), the ΔA^* of the $Ti_{51}Ni_{47}Si_2$ alloy ($\Delta A^* = 96$°C) is larger than that of $Ti_{51}Ni_{49}$ alloy ($\Delta A^* = 82$°C) for the same 25% cold rolling. Fig. 7(b) shows that the increment of hardness at 25% cold rolling for $Ti_{51}Ni_{47}Si_2$ alloy ($\Delta Hv = 161$ *Hv*) is larger than that of $Ti_{51}Ni_{49}$ alloy ($\Delta Hv = 143$ *Hv).* This feature results from the as-annealed $Ti_{51}Ni_{47}Si_2$ alloy being harder than $Ti_{51}Ni_{49}$ alloy due to Si atoms solute-soluted in the matrix. We propose that the dislocation/defect movement may be impeded more in $Ti_{51}Ni_{47}Si_2$ alloy than in $Ti_{51}Ni_{49}$ alloy and causes the harder $Ti_{51}Ni_{47}Si_2$ alloy to have a higher martensite stabilization under the same degree of cold rolling, as shown in Fig. 7.

3.4. The thermal cycling effect

Fig. 8 shows peak temperatures *M**, *A** and hardness *Hv* versus thermal cycle *N* for the annealed $Ti_{51}Ni_{47}Si_2$ alloy. In Fig. 8, the *M** and *A** temperatures decrease, but the hardness *Hv* increases with increasing *N*. It has been proposed that this feature comes from the dislocations induced by thermal cycling [1]. The *A** and *M** decrease quickly for the first 10 cycles with the decrement being about 16°C at $N = 10$, which is larger than that of $Ti_{51}Ni_{49}$ alloy ($\cong 10$°C at $N = 10$) [20]. The increase in hardness of this alloy ($\Delta Hv = 28$) is also greater than that of $Ti_{51}Ni_{49}$ alloy ($\Delta Hv = 19$) at the same $N = 10$ cycles. This difference indicates that $Ti_{51}Ni_{47}Si_2$ alloy can induce more dislocations than $Ti_{51}Ni_{49}$ alloy in the early thermal cycling. We suggest that the volume change during the martensitic transformation can induce complex stress fields at the interface of second phase particles and B2/B19′ matrix during thermal cycling. These complex stress fields may enhance the dislocation multiplication, and therefore, increase the hardness of the alloy and depress its *M** and *A** temperatures. In Fig. 8, after 50 cycles, the *A** and *M** temperatures reach constant values. This indicates that the quantities of induced dislocations reach a saturated value after 50 cycles in $Ti_{51}Ni_{47}Si_2$ alloy.

3.5. Strengthening effects of cold-rolling and thermal cycling on martensitic transformation temperatures

Fig. 9(a) and (b) show the curves of peak temperature *M** versus hardness *Hv* for the cold-rolled and thermal-cycled $Ti_{51}Ni_{47}Si_2$ alloy, respectively. The results of cold-rolled and thermal-cycled $Ti_{51}Ni_{49}$ alloy are also shown in Fig. 9. It was pointed out that any strengthening mechanism which impedes the transformation shear can lower the transformation temperatures because the martensitic transformation involves a shear process [26,27]. This feature can be expressed by Eq. (1).

Table 2
DSC measurement and hardness test of $Ti_{51}Ni_{47}Si_2$ alloy at various thickness reductions

Thickness reduction (%)	A_1^* (°C)	ΔH_{h1} (J/g)	M_1^* (°C)	ΔH_C (J/g)	A_2^* (°C)	ΔH_{h2} (J/g)	Hardness (*Hv*)
0	114	27.9	74	27.2	107	26.3	245
5	134	23.2	61	19.8	101	20.4	284
10	150	18.6	50	14.8	96	16.5	321
20	165	12.4	36	10.7	81	11.7	371
25	171	9.2	28	8.2	75	7.9	406

$$M_s = T_o - K\Delta\sigma_y \quad (1)$$

where the constant K contains the factors of proportionality between the critical shear stress and the yield stress $\Delta\sigma_y$, the equilibrium temperature T_o is a function of the chemical composition, and the yield stress $\Delta\sigma_y$ is regarded as proportional to the hardness.

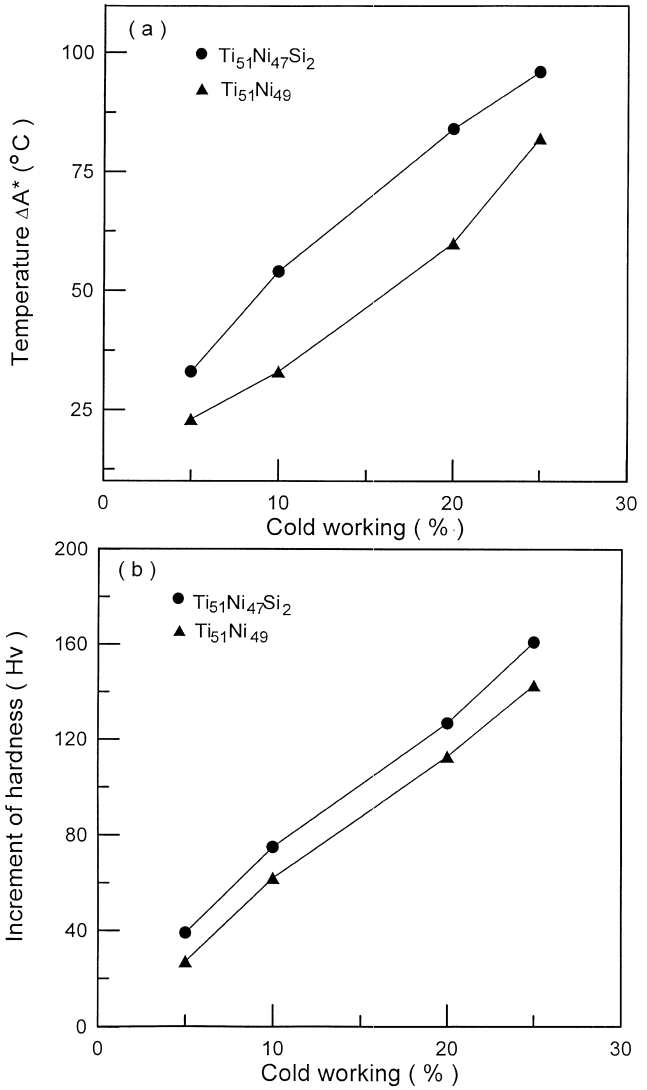

Fig. 7. (a) The degree of martensite stabilization (ΔA^*) and (b) the increment of hardness (ΔHv) versus the degree of cold rolling for the $Ti_{51}Ni_{47}Si_2$ alloy.

In this study, both cold-rolling and thermal cycling do not change the alloy's composition, hence T_o is a constant. In addition, both cold rolling and thermal cycling can strengthen the alloys by inducing dislocations, and therefore can raise the yield stress $\Delta\sigma_y$. As derived from Eq. (1), both cold-rolling and thermal cycling should cause the M^* and A^* temperatures to be lowered by the strengthening effect. This prediction is qualitatively consistent with the results of Fig. 9. In Fig. 9, the slope represents the constant K, which is not the same for different strengthening processes. As mentioned above, strengthening processes can introduce dislocations in alloys. However, dislocations induced by cold rolling come from the plastic deformation of martensite and those induced by thermal cycling come from the thermal stress and transformation shear associated with B2↔B19. Carefully examining Fig. 9, the constant K of $Ti_{51}Ni_{47}Si_2$ alloy is larger than that of $Ti_{51}Ni_{49}$ alloy for the same strengthening process. We propose that the K value is related to the inherent hardness of the annealed TiNi or TiNiX alloys and the depression of $M_s(M^*)$ and $A_s(A^*)$ temperatures by the strengthening mechanism is stronger for the alloy having a higher annealed hardness. $Ti_{51}Ni_{47}Si_2$ alloy has a higher inherent hardness than $Ti_{51}Ni_{49}$ alloy owing to Si atoms solid-soluted in TiNi alloy. This elucidates why, for the same strengthening mechanism, $Ti_{51}Ni_{47}Si_2$ alloy has higher K values than $Ti_{51}Ni_{49}$ alloy, as observed in Fig. 9.

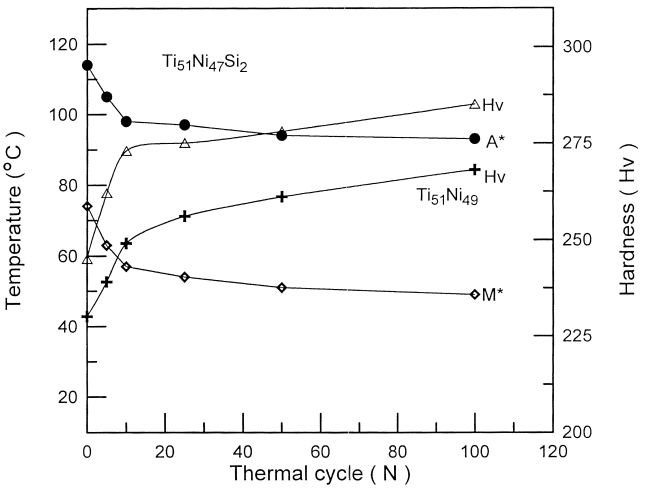

Fig. 8. Peak temperatures A^* and M^* and hardness Hv versus the number of thermal cycles N for the $Ti_{51}Ni_{47}Si_2$ alloy.

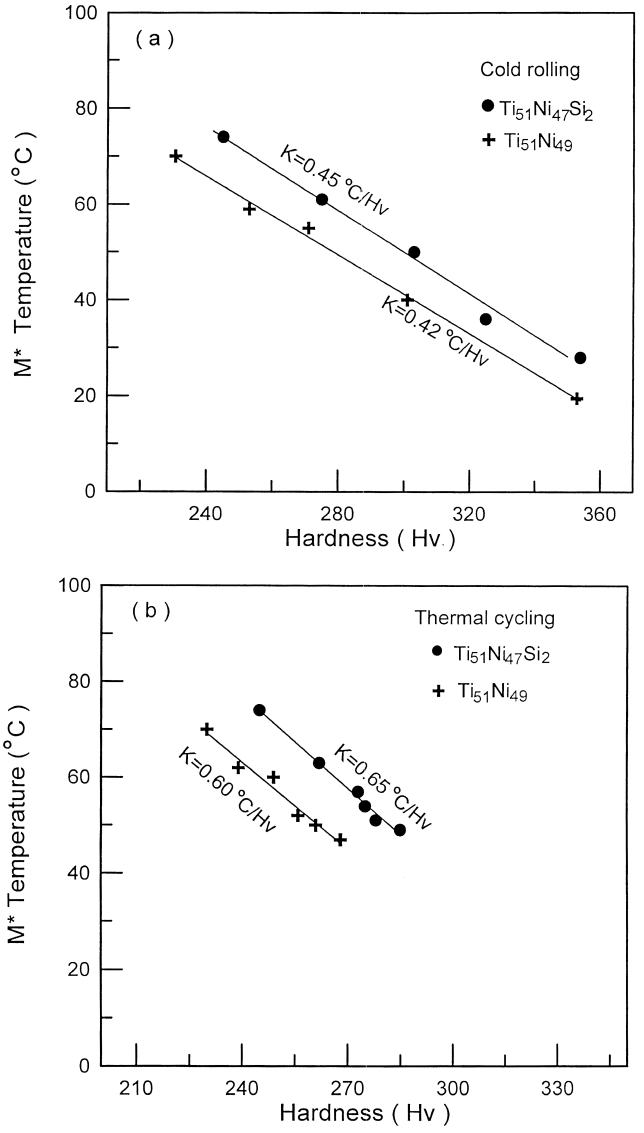

Fig. 9. M^* temperature versus hardness Hv for (a) cold-rolled and (b) thermal cycled $Ti_{51}Ni_{47}Si_2$ and $Ti_{51}Ni_{49}$ alloys.

4. Conclusion

The annealed $Ti_{51}Ni_{47}Si_2$ alloy undergoes the one-stage B2↔19′ martensitic transformation and its transformation temperatures are nearly equal to those of as-annealed $Ti_{51}Ni_{49}$ alloy. Many second phase particles are formed around the grain boundaries of the matrix in which the matrix is Ti(Ni,Si) phase and the second phase particles are Ti_2(Ni,Si) and χ phases. Despite the existence of many particles, this alloy still exhibits good shape recovery. The B19′ martensite structure in $Ti_{51}Ni_{47}Si_2$ alloy is calculated from the SADPs as $a=0.284$ nm, $b=0.412$ nm, $c=0.468$ nm and $\beta=98°$.

Transformation temperatures decrease and hardness increases with increasing aging time at 400°C. This characteristic may be related to the aging effects of point defects/atom rearrangements in B2 phase. The fine plates of $(001)_M$ compound twins are easy to form for the aged specimens.

Martensite stabilization can be induced by cold rolling at room temperature. The hardness increment of this alloy is more than that of $Ti_{51}Ni_{49}$ alloy under the same degree of cold rolling. Si atoms solid-soluted in TiNi alloy is suggested to account for this characteristic.

A^* and M^* temperatures decrease and the hardness increases in the first 10 cycles of thermal cycled $Ti_{51}Ni_{47}Si_2$ alloy. Meanwhile, the decrement of A^* temperatures of this alloy is larger than that of $Ti_{51}Ni_{49}$ alloy at the same N due to the former alloy having a harder matrix.

The strengthening effects of cold-rolling and thermal cycling on $M_s(M^*)$ temperature of $Ti_{51}Ni_{47}Si_2$ alloy are found to follow the equation $M_s=T_o-K\Delta\sigma_y$. Strengthening processes of cold rolling and thermal cycling have different K values. The annealed hardness of $Ti_{51}Ni_{47}Si_2$ alloy is higher than that of $Ti_{51}Ni_{49}$ alloy and causes the former alloy to have a higher K value than the latter under the same strengthening process.

Acknowledgements

The authors are pleased to acknowledge the financial support of this research by the National Science Council (NSC), Republic of China under Grants NSC 88-2216-E002-013 and NSC 89-2216-E151-010.

References

[1] S. Miyazaki, Y. Igo, K. Otsuka, Acta Metall. 34 (1986) 2045.
[2] S.K. Wu, H.C. Lin, T.S. Chou, Acta Metall. 38 (1990) 95.
[3] M. Nishida, T. Honma, Scripta Metall. 18 (1984) 1293.
[4] M. Nishida, T. Honma, Scripta Metall. 18 (1984) 1299.
[5] H.C. Lin, S.K. Wu, T.S. Chou, H.P. Kao, Acta Metall. 39 (1991) 2069.
[6] K.H. Eckelmeyer, Scripta Metall. 10 (1976) 667.
[7] R. Wasilewski, in: J. Perkin (Ed.), Shape Memory Effects in Alloys, Plenum, New York, 1975, p. 245.
[8] V.I. Kolomystev, Scripta Metall. 31 (1994) 1415.
[9] C.M. Hwang, M. Meichle, M.B. Salamon, C.M. Wayman, Phil. Mag. 47A (1983) 177.
[10] S.K. Wu, C.M. Wayman, Metallography 20 (1987) 359.
[11] Y.C. Lo, S.K. Wu, C.M. Wayman, Scripta Metall. 24 (1990) 1571.
[12] P.G. Lindqist, C.M. Wayman, in: T.W. Duering, K.N. Melton, D. Stockel, C.M. Wayman (Eds.), Engineering Aspects of Shape Memory Alloys, Butterworth–Heinemann, London, 1990, p. 58.
[13] C.M. Hwang, C.M. Wayman, Scripta Metall. 17 (1983) 1345.
[14] K.R. Edmonds, C.M. Hwang, Scripta Metall. 20 (1986) 733.
[15] X. Ren, N. Mirua, K. Taniwaki, K. Otsuka, T. Suzuki, K. Tanaka, Y.I. Chumltyakov, M. Asai, Mater. Sci. Eng. A273–275 (1999) 190.
[16] Y.C. Lo, S.K. Wu, H.E. Horng, Acta Metall. Mater. 41 (1993) 747.
[17] J.Z. Chen, S.K. Wu, Thin Solid Films 339 (1999) 194.
[18] S.K. Wu, J.Z. Chen, Y.J. Wu, J.Y. Wang, M.N. Yu, F.R. Chen, J.J. Kai, Phil. Mag. A 81 (2001) 1939.
[19] M. Nishida, C.M. Wayman, T. Honma, Metall. Trans. 17A (1986) 1505.

[20] H.C. Lin, S.K. Wu, J.C. Lin, Mater. Chem. Phys. 37 (1994) 184.
[21] H.C. Lin, S.K. Wu, Scripta Metall. 26 (1992) 59.
[22] V.Y. Markiv, E.I. Gladyshevskii, P.I. Kripyakevich, T.I. Fedoruk, Inorg. Mater. 2 (1966) 1126.
[23] S.F. Hsieh, S.K. Wu, J. Mater. Sci. 34 (1999) 1659.
[24] S.K. Wu, S.F. Hsieh, J. Alloys Comp. 297 (2000) 294.
[25] R. Santamarta, C. Segui, J. Pons, E. Cesari, Scripta Mater. 41 (1999) 867.
[26] M. Cohen, E.S. Machlin, V.G. Paranjpe, in: Thermodynamics in Physical Metallurgy, ASM, Metals Park, OH, 1950, p. 242.
[27] E. Hornbogen, Acta Metall. 33 (1991) 595.